

K-band polarimetry of seven high-redshift radio galaxies

G. Leyshon^{1,2} and Stephen A. Eales^{1,3}

¹*Department of Physics and Astronomy, University of Wales Cardiff, P.O. Box 913, Cardiff CF2 3YB*

²*G.Leyshon@astro.cf.ac.uk*

³*S.Eales@astro.cf.ac.uk*

30 September 2018

ABSTRACT

We present the results of K-band imaging polarimetry of seven 3CR radio galaxies with $0.7 < z < 1.2$. We find strong evidence for polarization in three sources: 3C 22, 3C 41 and 3C 114. Of these, 3C 41 shows strong evidence of having a quasar core whose infrared light is scattered by dust. We also find some evidence for polarization in 3C 54 and in 3C 356. The two pointlike sources (3C 22 and 3C 41) and the barely-elongated 3C 54 appear to have of order ten per cent of their K-band flux contributed by scattered light from the active nucleus. We conclude that scattered nuclear light can form a significant component of the near-infrared light emitted by high-redshift radio galaxies, and discuss models in which the scattering particles are electrons and dust-grains.

Key words: infrared: galaxies – polarization – galaxies: active

1 INTRODUCTION

A popular model for high-redshift radio galaxies was proposed by Lilly & Longair (1984) a decade ago. Their study of the K- z Hubble diagram for 3CR radio galaxies showed a tight correlation: the K-magnitudes exhibit a constant dispersion up to $z \gtrsim 1$, but there is evolution with redshift such that galaxies at $z \sim 1$ are about 1 mag more luminous than at $z = 0$. Such a result is explicable if the observed K-band light originates in stars, and radio galaxies undergo a burst of star formation at a very early epoch, followed by passive evolution. A similar model has been suggested for radio-quiet elliptical galaxies (Eggen, Lynden-Bell & Sandage 1962).

This model for radio galaxies was challenged by two discoveries, which suggested that a significant part of the optical light originated in the active nucleus rather than the host galaxy. It was found that optical light from high- z radio galaxies is usually aligned with the radio axis (Chambers, Miley & van Breugel 1987; McCarthy et al. 1987) – the so-called ‘alignment effect’ – and that the optical light is often polarized with its \mathbf{E} -vector oriented perpendicular to the radio axis (di Serego Alighieri et al. 1989; Jannuzi & Elston 1991; Tadhunter et al. 1992). The polarization of the optical light suggests that it is emitted in a restricted range of directions by the active nucleus, and has been scattered into our line of sight, by either dust or electrons.

Lilly & Longair’s (1984) model may still be correct if the optical light originates in the active core while the (observer’s frame) K-band light comes from stars in the host galaxy. One test of this is whether the alignment effect ex-

tends to the near-infrared; Dunlop & Peacock (1993) find a clear infrared/radio alignment effect for a sample of 3CR radio galaxies – consistent with the smaller 3C sample of Rigler et al. (1992), which suggested that an infrared alignment effect was present, but weak.

Eales et al. (1997) compared the infrared luminosity of 3CR galaxies with that of a sample of B2/6C galaxies (selected for their lower radio intensities in approximately the same frequency band as the 3CR galaxies). They found that B2/6C galaxies are fainter than 3C galaxies at similar redshifts, by 0.6 mags in K-band at $z \sim 1$; their sample also confirms Dunlop & Peacock’s (1993) finding that the infrared alignment effect is strongest in sources with high radio luminosity. Eales et al. (1997) argue, therefore, that part of the infrared luminosity of radio galaxies arises from the active nucleus, and so a selection effect will produce the strong alignment effect and brighter K-band magnitudes observed in the most radio-luminous galaxies, *viz.* 3C galaxies at high z . One possible explanation of this result is that a significant fraction of a radio galaxy’s infrared light emerges from the active nucleus in a restricted cone, and enters our line of sight after scattering by dust or electrons. There is already other evidence that light from the active nucleus, if not necessarily scattered, can dominate the K-band light from high- z radio galaxies: Dunlop & Peacock (1993) noted that radio galaxy 3C 22 appeared to be exceptionally round and bright, and spectroscopic studies by Rawlings et al. (1995) confirmed that in the K-band, 3C 22 has properties more similar to those of a quasar than of a radio galaxy.

We have started a programme of near-infrared polarimetry for two reasons. Detection of infrared polariza-

arXiv:astro-ph/9708085v1 8 Aug 1997

Table 1. Redshifts and integration times for our sample of radio galaxies.

Source	IAU form	z	$\lambda_r(\mu\text{m})$	$t_{\text{int}}(\text{min})$
3C 22	0048+509	0.936	1.14	72
3C 41	0123+329	0.794	1.23	108
3C 54	0152+435	0.827	1.20	135
3C 65	0220+397	1.176	0.92	72
3C 114	0417+177	0.815	1.21	189
3C 356	1723+510	1.079	1.06	99
3C 441	2203+292	0.707	1.29	144

Key: z : redshift; λ_r : rest-frame equivalent of observed-frame $2.2\mu\text{m}$; t_{int} : total integration time summed over all waveplate settings.

tion would reinforce the evidence that scattered non-stellar light makes a significant contribution to the infrared in radio galaxies. Also, K-band polarimetry provides a valuable complement to optical polarimetry: a long wavelength baseline allows a more powerful test of whether the scattering centres are electrons, with a wavelength-independent scattering cross section, or dust, which preferentially scatters short wavelengths (Cimatti et al. 1993).

2 OBSERVATIONS AND REDUCTION PROCEDURE

2.1 Our sample

We observed a sample of seven high-redshift 3C radio galaxies at redshifts $0.7 < z < 1.2$. These form a representative sample of the different morphologies present in this redshift band: 3C 22 and 3C 41 are bright and appear pointlike; 3C 114 and 3C 356 display complex knotted morphologies with large scale alignments between the K-band structure and the radio axis; 3C 54, 3C 65 and 3C 441 are faint sources with some indication of K-band structure. Of these three faint sources, 3C 54 displays an alignment between the K-band morphology and the radio axis (Dunlop & Peacock 1993), 3C 65 shows no preferred direction in its H-band structure (Rigler & Lilly 1994), and 3C 441 has a broad-band optical polarization which is roughly perpendicular to its radio structure (Tadhunter et al. 1992). Table 1 lists the sources observed with their redshifts and the rest-frame wavelength of the observed light.

2.2 Instrumentation

We had the first run after the commissioning run of a new instrument, IRPOL2, installed at UKIRT (the United Kingdom Infrared Telescope, Hawaii). The IRPOL2 polarimeter consists of a rotatable half-wave plate and a Wollaston prism, working in conjunction with the IRCAM3 InSb array detector. We used IRCAM3 at the default pixel scale, 0.286 arcsec/pixel (Aspin 1994), with a K-band filter. The Wollaston prism causes each source in its field of view to appear as a pair of superimposed images with orthogonal polarizations, separated by -0.93 pixels in right ascension and $+69.08$ pixels in declination (Aspin 1995).

The design of the instrument is such that when the

waveplate is set to its 0° reference position, an object totally linearly polarised with its electric vector at 83° (i.e. celestially East of North) would appear only in the upper (Northern) image, and an object totally linearly polarised at -7° would only appear in the lower image. There are four standard offset positions for the waveplate: 0° , 22.5° , 45° and 67.5° . The IRPOL2 system has negligible instrumental polarization (Hough, private communication; Chrysostomou 1996). We took data on the nights of 1995 August 25, 26, and 27.

2.3 Observing procedure

For each target object, we took a ‘mosaic’ of nine images with the waveplate at the 0° offset. One image consisted of a 60 second exposure (the sum of six ten-second co-adds), and the mosaic was built up by taking one image with the target close to the centre, and eight images with the frame systematically offset from the first by ± 28 pixels (8 arcsec) horizontally and/or vertically. The same source was then similarly observed with the waveplate at the 22.5° , 45° and 67.5° offsets, completing one cycle of observations; hence one such cycle took 36 minutes of integration time. Between two and five observation cycles were performed over the three nights for each target; the total integration time for each target is given in Table 1. The times quoted are not exact multiples of 36, as in some cases, mosaics were corrupted by problems with the windblind, and excluded from our analysis. An example of a mosaic, 3C 54 and its surrounding field, observed with the waveplate at 22.5° , is shown in Figure 1.

2.4 Data reduction

We reduced the data by marking bad pixels, subtracting dark frames, and flat-fielding. Flat-fielding frames were obtained by median-combining the nine images of each mosaic without aligning them, and normalizing the resulting image by its mean pixel value. In order to align each set of nine images, we chose a star present on each frame, and measured its position with the APPHOT.CENTER routine in the IRAF package. Using these positions, the nine images were melded into a single mosaic image.

We performed photometry on the pairs of images of field stars and of radio galaxies in each mosaic using APPHOT.PHOT from the IRAF package. For each target, we chose one mosaic arbitrarily to determine the best aperture. Using this mosaic, we performed photometry on the two images of the source at a series of radii increasing in unit pixel steps. The measured magnitude in each aperture decreases as the light included in the aperture increases; we found the first pair ($r, r + 1$) of radii where the change in magnitude was less than half the measured error on the magnitude. We then used the photometry at the next radius, ($r + 2$). In this way, we hope to include all the source light but as little as possible of the surrounding sky. Where the chosen apertures differed for the two images of the source, we adopted the larger. The chosen aperture was then used on all the mosaics containing the target to obtain a set of intensities at the corresponding waveplate positions.

The APPHOT.PHOT routine corrects for the sky brightness by measuring the modal light intensity in an annulus

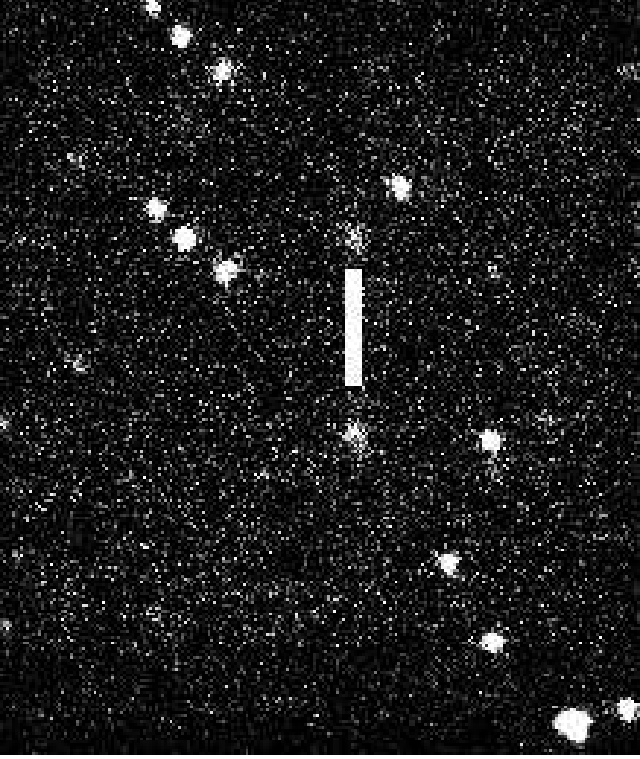


Figure 1. K-band image of 3C 54 (at either end of the bar) and surrounding field. (North is at the top, East at the left. The image was composed by mosaicing a series of nine 60-second exposures taken with the waveplate offset at 22.5° .)

around the target; the position of the annulus was chosen in each case such that the outer radius did not extend to the nearest neighbouring object, and the inner radius was normally set one pixel greater than the photometry aperture. (Where we attempted to perform photometry on a knot within a larger structure, the inner radius of the annulus was set sufficiently large to exclude all the knots comprising the object.) This procedure results in pairs of photometric intensities for each target.

2.5 Confidence intervals for polarization

Using the photometric intensities from all the observing cycles, we pooled the data and calculated the intensity-normalised Stokes Parameters, q and u , following the method of Clarke et al. (1983). The q and u (as quoted in Table 3) are in the instrumental reference frame, such that a positive q and zero u would indicate polarization at 83° East of North: q is defined by subtracting the lower beam intensity from the upper with the waveplate at the 0° reference position, and u similarly with the waveplate at 22.5° . The Stokes Parameters were then used to derive a measured degree of polarization, $p = \sqrt{q^2 + u^2}$.

Since p is positive in the presence of noise even for an unpolarised source, there has been some debate about the best method of obtaining an ‘unbiased’ estimate of the polarization (Simmons & Stewart 1985; Leyshon 1997). Following best practice, we assume that the Stokes Parameters q and u are normally distributed, and that the errors on the two parameters are comparable. Under these assumptions,

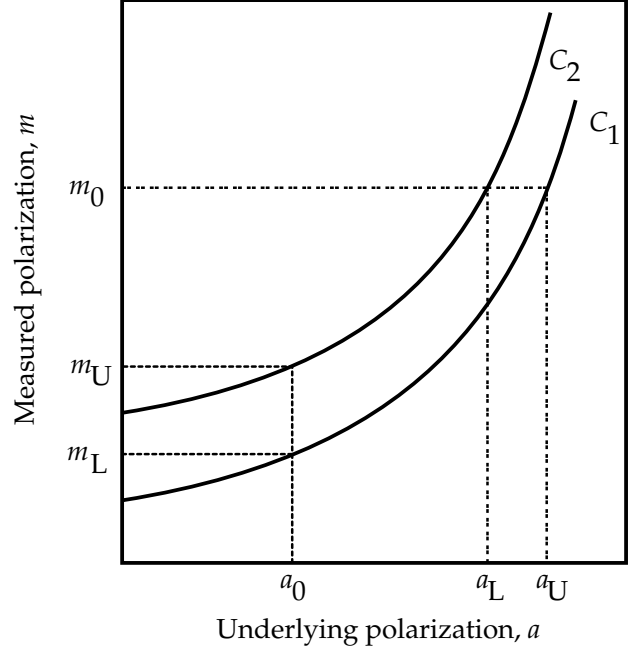


Figure 2. Illustration of contours in the $a - m$ plane. See text.

it can be shown (Wardle & Kronberg 1974; Vinokur 1965) that, if the underlying polarization of a source is p_0 and the error on a measurement is σ , then the probability distribution function for the measured polarization values p will be a Rice distribution. Defining normalised variables $a = p_0/\sigma$ and $m = p/\sigma$, we can write this distribution as

$$F(m, a) = m \cdot \exp\left[\frac{-(a^2 + m^2)}{2}\right] \cdot I_0(ma) \quad (1)$$

where $m \geq 0$ and I_0 is the modified Bessel function. It follows, trivially, that the integral

$$\int_{m=0}^{m=m_C(a)} F(m, a) \cdot dm = C \quad (2)$$

for $0 \leq C \leq 1$ represents a confidence interval $(0, m_C)$ such that there is a chance C of a measurement of the polarization lying within these bounds.

We need to invert the probability distribution to estimate a given our measured m . Following the method of Mood, Graybill & Boes (1974) we can solve Equation 2 for m_C for given values of C and a , and so plot contours of constant C on the $a-m$ plane, as illustrated in Figure 2. Clearly two contours C_1, C_2 allow us to read off a $C_2 - C_1$ confidence interval (m_L, m_U) for given a_0 . Mood et al. (1974, Ch. VIII, §4.2) show that the same contours also provide a $C_2 - C_1$ confidence interval for the underlying polarization (a_L, a_U) for a given measurement m_0 .

As well as providing a general interval (a_L, a_U) , the contours can be used to determine the probability that the underlying polarization is non-zero. The probability that $a = 0$ exactly is finite rather than infinitesimal, since some sources may be unpolarised. There will be some contour C_m , which cuts the m -axis at our measured m_0 , and so divides the domain of a into $a > 0$ with confidence C_m , and $a = 0$ with

confidence $1 - C_m$. This confidence can be found analytically, since Equation 2 can be integrated at $a = 0$; and it follows that the probability that $a > 0$, given some measured value m , is

$$C_m = 1 - \exp(-m^2/2). \quad (3)$$

Equation 3 can be used to determine the probability that a source is truly polarised, and the probabilities so derived for each source are listed in Table 3.

For a given measurement m_0 , it is also possible to use appropriate pairs of contours to find a set of 67 per cent (1σ) or 95 per cent (2σ) confidence intervals for our best estimate, \hat{a} . For any given required confidence, there will be a continuous set of pairs of contours which could be chosen; following Simmons & Stewart (1985) we choose the unique interval whose width is minimized by the additional constraint

$$F(m_L, a) = F(m_U, a). \quad (4)$$

The errors on the polarizations quoted in Table 3 are the 1σ errors derived by this method.

2.6 Point estimates for polarization

To obtain a point estimate of the polarization, we again follow Simmons & Stewart (1985), who have tested various estimators \hat{a}_X for bias. They find that when $a \lesssim 0.7$, the best estimator is the ‘Maximum Likelihood Estimator’, \hat{a}_{ML} ; when $a \gtrsim 0.7$, the best estimator, \hat{a}_{WK} , is that traditionally used by radio astronomers, e.g. Wardle & Kronberg (1974). It can be shown that $\hat{a}_{ML} < \hat{a}_{WK} \forall m$ (Simmons & Stewart 1985).

We do not know, *a priori*, whether a will be greater or less than 0.7, and hence which estimator to use. We distinguish three cases: (i) both estimators indicate $\hat{a}_X \lesssim 0.7$, so we must use \hat{a}_{ML} ; (ii) both estimators indicate $\hat{a}_X \gtrsim 0.7$, so we must use \hat{a}_{WK} ; or (iii) in the region of $\hat{a}_X \sim 0.7$, each estimator will indicate that it should be preferred over the other. We therefore wish to construct an estimator \hat{a} which is continuous with m and takes these cases into account. This can be done using the inequality $\hat{a}_{ML} < \hat{a}_{WK} \forall m$.

Case (i): Let m_{WKmin} be the measured value of polarization which would cause an estimate $\hat{a}_{ML} < \hat{a}_{WK} = 0.6$. Clearly if $m < m_{WKmin}$ then $\hat{a} < 0.7$ and the Maximum Likelihood estimator is certainly the most appropriate. We find that $m_{WKmin} = 1.0982$ (Leyshon 1997) and in this case, the Maximum Likelihood estimator will in fact be zero.

Case (ii): Let m_{MLmax} be the measured value of polarization which would cause an estimate $0.8 = \hat{a}_{ML} < \hat{a}_{WK}$. In this case, Wardle & Kronberg’s (1974) estimator will clearly be the most appropriate. We find that $m_{MLmax} = 1.5347$ (Leyshon 1997).

Case (iii): Between these two extremes, if our measured polarization satisfies $m_{WKmin} < m < m_{MLmax}$, we can interpolate such that our best estimate is

$$\hat{a} = \frac{m - m_{WKmin}}{m_{MLmax} - m_{WKmin}} \cdot \hat{a}_{ML} + \frac{m_{MLmax} - m}{m_{MLmax} - m_{WKmin}} \cdot \hat{a}_{WK}. \quad (5)$$

Thus we can obtain both a ‘debiased’ point estimate and a confidence interval for a , and hence for the degree of polarization $a\sigma$.

2.7 Estimating the angle of polarization

The position angle, $\phi = 83^\circ + \phi_m$, of the \mathbf{E} -vector is obtained by calculating

$$2\phi_m = \theta = \tan^{-1}(u/q), \quad (6)$$

and noting the appropriate quadrant from the signs of q and u . There are two methods of obtaining the error on this angle. We can propagate the errors on q and u through Equation 6, yielding an asymmetric error; or the symmetric 67 per cent confidence interval may be constructed, using the best estimate of a to calculate the relevant distribution function (Wardle & Kronberg 1974; Vinokur 1965). We calculated error bars by both methods, and selected the greater error in each case to quote in Table 3.

2.8 Extinction corrections

The interstellar medium may impose some linear polarization on light transmitted through it. Empirically, the polarization p depends on wavelength, such that

$$p/p_{max} = \exp[-1.7\lambda_{max} \ln^2(\lambda_{max}/\lambda)] \quad (7)$$

where λ_{max} is the wavelength (explicitly in micrometres) at which the polarization peaks, usually around $0.5\mu m$, and empirically in the range $0.3\text{--}0.8\mu m$ (Serkowski, Matthewson & Ford 1975; Wilking et al. 1980). The relationship is found to hold up to around $2\mu m$, and is adequate for our purposes (Martin & Whittet 1990).

In general, p_{max} for a given set of galactic co-ordinates is not known. But suppose we take the ratio of polarizations in two wavebands, V and K, and rearrange:

$$p_K = p_V \exp \left\{ -3.4\lambda_{max} \left[\ln \left(\frac{\lambda_{max}}{\sqrt{\lambda_K \lambda_V}} \right) \ln \left(\frac{\lambda_V}{\lambda_K} \right) \right] \right\}. \quad (8)$$

Hence $p_K = c p_V$ where c depends on λ_{max} but for $0.3 < \lambda_{max} < 0.8$ we find $0.15 < c < 0.30$.

An empirical upper limit for p_V (expressed as a percentage) is given by Schmidt-Kaler (1958) as $p_V \leq 9E_{B-V}$ and typically, $p_V = 4.5E_{B-V}$. It is well established (Savage & Mathis 1979; Koorneef 1983; Rieke & Lebofsky 1985) that the ratio of total to selective extinction is $A_V/E_{B-V} \sim 3$; and so we can use the extinctions A_B (Burstein & Heiles 1982, figures obtained from the NED database) to obtain $E_{B-V} = A_B - A_V = A_B/4$.

Taking the maximum values, $c = 0.3$ and $p_V \leq 9E_{B-V}$, we find an upper limit for infrared polarization $p_K \leq 0.7A_B$. The NED values for A_B and the corresponding upper limits on p_K are given in Table 2.

3 RESULTS

3.1 Have we detected polarization?

Equation 3 allows us to quantify the probability that a given object is polarised. The probabilities of each object being polarised are listed in Table 3. Three of our seven sources have a 95 per cent or better probability of being polarised; and of these, 3C 22 and 3C 41 are polarised at the 3 per cent level, and 3C 114 at the 12 per cent level.

The number of prominent starlike objects (in addition to the target) featuring on the mosaics varies between one

Table 2. Total B-band extinctions and upper limits on K-band interstellar polarization for our sample.

Source	A_B	$p_{K,\max}$
3C 22	1.09	0.76
3C 41	0.17	0.12
3C 54	0.37	0.26
3C 65	0.16	0.11
3C 114	1.26	0.88
3C 356	0.10	0.07
3C 441	0.34	0.24

Key: A_B : Blue-band extinction (magnitudes), from NED, derived from Burstein & Heiles (1982); $p_{K,\max}$: maximum interstellar contribution to K-band polarization (per cent) as described in the text.

and seven, depending on the target. Where possible, we have performed polarimetry on the stars; out of the 21 stars so observed, only one has a greater than 95 per cent probability of being polarised. This object was a bright starlike object on the mosaic containing 3C 114, but is only polarised at the 0.7 per cent level, which is explicable by the interstellar medium (see Table 2).

Within the bin of sources having a probability 80-95 per cent of being polarized, fall three further stars; of these, one is extremely faint, and another appears to be polarised at only the 0.3 per cent level. The third falls on the same mosaic as 3C 54, and appears to be polarised at the 5.6 ± 2.6 per cent level, with a 94 per cent chance of the polarization being genuine. This star, however, straddles the edge of three of the nine component frames of the mosaics, so the validity of the result is called into question. Two of our sources also fall in the 80-95 per cent probability bin: 3C 54 itself, polarised at the 6 per cent level, and 3C 356, at the 9 per cent level.

Given that 17 out of 21 stars, but only 2 out of 7 sources, have a probability of less than 80 per cent of being polarised at all, we feel confident of having detected polarization in three 3C sources, and possibly in a further two.

3.2 Individual objects

3C 22

3C 22 has a 95 per cent chance of truly being polarised, and the debiased polarization is 3.3 ± 1.4 per cent. We expect that no more than 0.8 per cent is due to the interstellar medium; most of the polarization is therefore intrinsic to the source. The orientation of the \mathbf{E} -vector is $+27_{-71}^{+17}$ East of North. Our K-band image shows no evidence for extended structure.

The radio position angle of 3C 22 is 102° (Schilizzi, Kapahi & Neff 1982). The errors on the measured polarization orientation are large, but the figures suggest that the true direction is more likely to be perpendicular to the radio axis, than parallel to it. As we have already seen, 3C 22 is suspected of being an obscured quasar (Dunlop & Peacock 1993; Rawlings et al. 1995); according to data in Lilly & Longair (1984), its K-band magnitude (15.67 ± 0.10) is brighter than the mean K- z relationship by about 0.9 mag. A perpendicular alignment of the radio axis and \mathbf{E} -vector orientation would be expected for light from the active nucleus travel-

ling along the radio axis and then scattered towards us by either dust or electrons. Jannuzi (private communication) (Elston & Jannuzi 1997) has performed imaging polarimetry on 3C22 at shorter wavelengths, and reports 3σ upper limits in V and H of 5 per cent and 3 per cent respectively.

3C 41

3C 41 has a 98 per cent chance of having an underlying polarization, which we measure to be 3.1 ± 1.1 per cent. Our upper limit for extinction-induced polarization is only 0.1 per cent, so we are confident of having detected intrinsic polarization in this object. The orientation of the \mathbf{E} -vector is $+45_{-14}^{+79}$ East of North. Our K-band image shows no evidence for extended structure. Like 3C 22, Lilly & Longair's (1984) data shows that, at $K = 15.95 \pm 0.10$, 3C 41 is significantly brighter than the mean K- z relationship, by about 0.6 mag.

Jannuzi (private communication) (Elston & Jannuzi 1997) have firm V and H band polarizations for this source: at V, the polarization is 9.3 ± 2.3 per cent at $+58^\circ \pm 7^\circ$; at H, the polarization is 6.6 ± 1.6 per cent at $+57^\circ \pm 7^\circ$. The \mathbf{E} -vector orientations in the three wavebands are consistent with one another. The radio position angle of 3C 41 is 147° (Longair 1975), so we have a very good perpendicular alignment between the radio and polarization axes.

3C 54

The probability that 3C 54 is polarised is 94 per cent; our measured value of polarization is 5.9 ± 2.6 per cent at $+32_{-79}^{+17}$ East of North. Dust is not expected to contribute more than 0.3 per cent. We have no independent polarimetry for this object. The position angle of its radio structure is 24° (Longair 1975); our measurement shows that the polarization orientation is more likely to be parallel to the radio axis, than perpendicular to it, but the latter case cannot be ruled out. Dunlop & Peacock's (1993) K-band contour map shows a slight extension to the south-west, which was also just discernible in our image. This would be roughly parallel with the radio axis.

3C 114

An image of 3C 114 is shown in Figure 3. It consists of at least four knots, where the brightest knot forms the knee of a Γ -shaped structure. Only the knee knot proved bright enough to analyze on its own; Table 3 includes results for both that knot and the structure as whole. There is a probability in excess of 99 per cent that there is genuine polarization in both the knee knot and the overall structure.

We measured polarization in the knee of 5.1 ± 1.7 per cent, at $+111_{-63}^{+14}$ East of North. Overall, the whole object has a polarization of 11.7 ± 3.0 per cent at $+73_{-20}^{+34}$. The extinction contribution could be as high as 0.9 per cent, but our detections of polarization are much higher than this, so the polarization appears to be intrinsic.

The radio position angle of 3C 114 is 54° (Strom et al. 1990). Our measurements of the \mathbf{E} -vector orientation suggest that an alignment parallel to the radio and optical axes

Table 3. Observational results from polarimetry of 7 radio galaxies in K-band.

Source	$q(\sigma_q)(\%)$	$u(\sigma_u)(\%)$	$r(\prime\prime)$	$P \pm \sigma_P(\%)$	2σ .UL	Prob	$\theta(^{\circ})$	$\sigma_{\theta}(^{\circ})$
3C 22	-1.3 (1.4)	-3.2 (1.4)	2.6	3.27 ± 1.38	-	0.95	27.0	-71.4 +16.9
3C 41	+0.8 (1.1)	-3.1 (1.1)	2.3	3.09 ± 1.11	-	0.98	45.4	-14.3 +78.6
3C 54	-1.4 (2.5)	-6.0 (2.5)	4.0	5.90 ± 2.55	-	0.94	31.6	-79.1 +17.3
3C 65	-4.3 (4.2)	-1.2 (4.0)	2.9	$2.15 \pm {}^L 4.49$	9.7	0.42	0.6	± 71.4
3C 114	+11.2 (3.1)	-4.1 (2.7)	3.6	11.74 ± 3.02	-	0.99	72.9	-20.6 +33.9
●Knee	+3.0 (1.6)	+4.3 (1.8)	1.7	5.11 ± 1.73	-	0.99	110.6	-63.2 +13.5
3C 356	-9.6 (4.9)	+3.5 (5.6)	4.0	9.04 ± 4.94	16	0.85	172.0	± 22.1
●North	-13.3 (7.9)	+4.6 (8.4)	2.3	13.02 ± 7.99	41	0.62	163.5	± 25.0
●SE	-10.1 (9.4)	-18.9 (16.7)	2.6	18.99 ± 15.31	24	0.78	23.9	-54.2 +33.0
3C 441	-1.7 (2.3)	-0.8 (2.3)	3.4	$1.04 \pm {}^L 2.35$	4.7	0.26	6.2	± 77.3

Key: $q \pm \sigma_q, u \pm \sigma_u$: normalized Stokes Parameters (per cent) with respect to 83° E of N; r : radius of photometry aperture (arcseconds); $P \pm \sigma_P$: percentage polarization (debiased) with 1σ error (L — the 1σ lower limit for polarization is zero); Prob: the probability that there is underlying polarization, given by Equation 3; 2σ .UL: 2σ upper limit (in per cent) for polarization in objects unlikely to be polarised; $\theta \pm \sigma_{\theta}$: Electric vector orientation E of N ($^{\circ}$).

**Figure 3.** K-band structure of 3C 114. (North is at the top, East is on the left.)

is more likely than a perpendicular alignment, but the errors do not permit a more definite conclusion.

3C 356

We have no strong evidence for polarization in 3C 356, but we note that the structure has three lobes in its K-band image, at the North, the South-East and the South-West. Only the North and South-East knots were bright enough to permit polarimetry, as recorded in Table 3.

4 DISCUSSION

4.1 The fractional contribution of quasar light

Radio galaxies are thought to have quasar nuclei at their cores, but to be oriented such that no direct radiation from the core can reach us. Nearby radio galaxies are known to have the morphology of giant ellipticals; if this is also true at higher redshifts, the stellar populations of our seven sources will consist of mostly old, red, stars. The total light received from our sources will be a combination of starlight, light from the active nucleus scattered into our line of sight, and nebular continuum emission.

We denote by Φ_W , the fraction of the total flux density, F_W , in a given waveband, W , which originates in the active nucleus. We expect that in the visible wavebands, $\Phi_{U,B,V}$ will be a significant fraction of unity. From our observations, we wish to determine whether Φ_K is small, or whether a significant component of the stellar-dominated infrared also arises in the active nucleus.

Where the magnitude, W , has been measured in a given waveband, the total flux density can be calculated:

$$F_W = F_0(W=0).10^{-0.4W}, \quad (9)$$

if we denote the flux density scattered into our line of sight from the quasar core by $F_{Q,W}$, then $\Phi_W = F_{Q,W}/F_W$.

The optical flux density of quasars can be modelled well by a power law of the form $C.\nu^{-\alpha}$ where α , the ‘spectral index’, is of order unity. Since the efficiency with which a given species of scattering centre scatters light may depend on wavelength, we denote that efficiency by f_W , and the scattered quasar component can be expressed

$$F_{Q,W} = C.f_W.\nu^{-\alpha}. \quad (10)$$

It will be computationally convenient to define an ‘unscaled model light ratio’, ϕ_W , as

$$\phi_W = \frac{f_W.\nu^{-\alpha}}{F_0(W=0).10^{-0.4W}}; \quad (11)$$

then the actual model light ratio will be $\Phi_W = C.\phi_W$. There is clearly an upper limit set on C by the fact that Φ_W may not exceed unity in any waveband; hence $C \leq 1/\phi_W$. To allow for errors in the observed magnitudes, ΔW , the max-

imum permissible value of C in a model can be taken to be

$$C_{\max} = \min \left[\frac{F_0(W=0) \cdot 10^{-0.4(W-\Delta W)}}{f_W \cdot \nu^{-\alpha}} \right], \forall W, \quad (12)$$

where the value for α and the choice of scattering centre (hence of f_W) depend on the model.

4.2 The dilution law for polarization

Following Manzini & di Serego Alighieri (1996) (hereafter MdSA) we assume that only the scattered component of the light from radio galaxies is polarised. It can readily be shown that when linearly polarised light is mixed with unpolarised light, the overall degree of polarization is directly proportional to the fraction of the total intensity contributed by the polarised component. Hence defining $P_{Q,W}$ as the intrinsic polarization produced by the scattering process, and P_W as the observed polarization after dilution, it follows that

$$\Phi_W = F_{Q,W}/F_W = P_W/P_{Q,W}. \quad (13)$$

If we know the restrictions on possible values of the intrinsic polarization $P_{Q,W}$, we can use our corresponding measurements of P_W to put limits on Φ_W for the measured sources. The appropriate restrictions depend on the nature of the scattering centres.

If the scattering centres are electrons (Fabian 1989), then Thomson scattering will take place: the effects of the geometry and of the wavelength can be treated independently. The spectral energy distribution of the light scattered in a given direction is independent of the scattering angle: $P_{Q,W} = P_Q$ will be a constant. The degree of polarization of the scattered light is given simply by

$$P_Q = \frac{1 - \cos^2 \chi}{1 + \cos^2 \chi}, \quad (14)$$

where χ is the scattering angle. For an AGN observed as a radio galaxy, we assume an orientation $45^\circ \leq \chi \leq 90^\circ$, whence $1/3 \leq P_Q \leq 1 \forall W$.

The case where the scattering centres are dust grains has been modelled recently (MdSA); the fraction of the light scattered by the dust, f_W , and the polarization of the scattered light, $P_{Q,W}$, both depend strongly on wavelength. The exact relationship depends critically on the size distribution of the dust grains, and the amount of extinction they introduce; MdSA provide a series of graphs for the variation of f_W and $P_{Q,W}$ with rest-frame wavelength $0.1 \mu\text{m} < \lambda_r < 1.0 \mu\text{m}$, corresponding to many different dust grain compositions and size distributions. At the redshifts of the objects in our sample, the light observed in the H and J bands originated at rest-frame wavelengths below $1.0 \mu\text{m}$, but the K-band light originated in the region $1.0 \mu\text{m} < \lambda_r < 1.15 \mu\text{m}$. To accommodate the K-band light within our models, we linearly extrapolated MdSA's curves to $\lambda_r = 1.15 \mu\text{m}$.

In models where the smallest dust grains have a radius not less than 40 nm, $P_{Q,W}$ approaches zero twice: once at a (rest frame) wavelength around $0.2 \mu\text{m}$, and again at some wavelength between 0.1 and $0.7 \mu\text{m}$ which depends critically on the dust grain size distribution. But in all cases, $P_{Q,W}$ extrapolated into the $1.0 \mu\text{m} < \lambda_r < 1.15 \mu\text{m}$ region gives

Table 4. Percentage of K-band light estimated to be arising from the active nucleus in the 5 polarized galaxies.

Source	P_K	Φ_{K_e}	Φ_{K_d}
3C 22	3.3 ± 1.4	7 ± 4	8 ± 4
3C 41	3.1 ± 1.1	6 ± 4	8 ± 3
3C 54	5.9 ± 2.6	12 ± 8	15 ± 7
3C 114	11.7 ± 3.0	23 ± 13	29 ± 10
3C 356	9 ± 5	18 ± 13	23 ± 13

Key: P_K : measured K-band polarization; Φ_{K_e} : fraction of light from quasar according to electron model; Φ_{K_d} : fraction of light from quasar according to dust model. Depolarization from multiple scattering (both models), and shallower scattering angles (dust model only) will tend to increase Φ_K . The polarizations used for the compound objects 3C 114 and 3C 356 are those for the whole compounds.

$0.3 < P_{Q,K} < 0.5$; the intrinsic polarization at V and H is lower.

For the five sources in which we have evidence of K-band polarization, we can hence estimate Φ_K under both electron and dust models. The values are given in Table 4. For the dust models, we take $1/P_{Q,W} = 2.5 \pm 0.5$; the error takes into account all dust models, and the different redshift corrections for the different galaxies, but assumes that the scattering angle is 90° . If the scattering angle is less, we assume that less polarization occurs (see MdSA, Figure 20), and hence Φ_K will be greater than our estimate. For the electron models, we multiply the observed polarization by $1/P_{Q,W} = 2 \pm 1$; this takes into account all possible orientation effects.

The effects of multiple scattering have been ignored for both models; multiple scattering tends to depolarise light, and so the true value of Φ_K under multiple scattering will again be greater than our estimate. The only physical mechanism which could cause Φ_K to be *lower* than our estimate, is polarization of light in transit by selective extinction; and as we have already seen (Table 2), any such contribution to the polarization will be small.

4.3 Modelling the polarization of radio galaxies

Given a measurement of the magnitude of a radio galaxy, we can predict its polarization as a function of wavelength, up to a multiplicative constant. Rearranging Equation 13, and employing our ‘unscaled model light ratio’, we first define an ‘unscaled model polarization’ $\Pi_W = P_{Q,W} \cdot \phi_W$, and so express our modelled polarization as:

$$P_{W,\text{modelled}} = P_{Q,W} \cdot \Phi_W = C \cdot P_{Q,W} \cdot \phi_W = C \cdot \Pi_W. \quad (15)$$

To fit a dust scattering model, we can calculate Π_W by obtaining f_W and $P_{Q,W}$ from suitable curves in MdSA. For electron models, the wavelength-independent term f_W can be considered to have been absorbed into the multiplicative constant, C , while P_Q , also wavelength-independent, can be assumed to be its minimum value, $1/3$. We cannot separately identify C and P_Q ; the physical constraints on these constants are $1/3 \leq P_Q \leq 1$ and $0 \leq C \leq C_{\max}$. If P_Q is greater than the assumed $1/3$, then C will be correspondingly smaller.

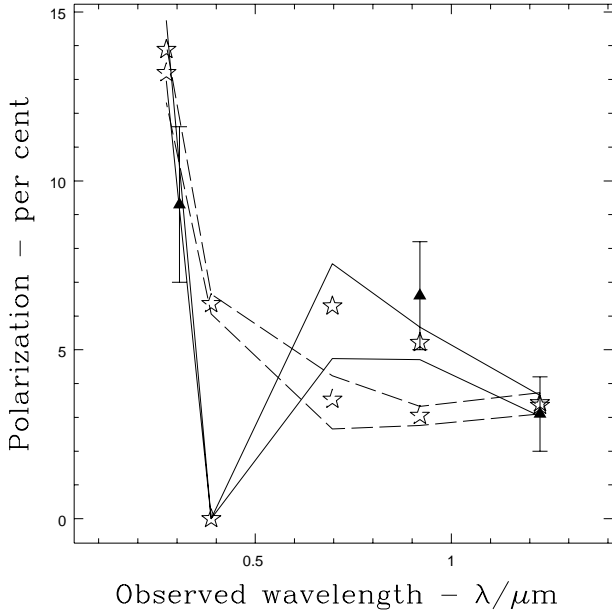


Figure 4. Measured and best-fit model polarizations of 3C 41 as a function of rest-frame wavelength. Solid line: dust model, $\alpha = 1.167$; dashed line: electron model, $\alpha = 1.733$.

Given a set of N polarization measurements $P_W \pm \sigma_W$, and a corresponding set of unscaled model polarizations, $\Pi_W \pm \epsilon_W$, based on measured magnitudes, we can calculate the deviation of the fit:

$$\delta = \sqrt{\frac{1}{N} \sum_{W_1 \dots W_N} \frac{(P_W - C \cdot \Pi_W)^2}{\sigma_W^2 + (C \cdot \epsilon_W)^2}}. \quad (16)$$

The best fit is that with the value of C which minimizes δ , subject to the physical constraint $0 \leq C \leq C_{\max}$.

A model for 3C 41

The source for which we had the most data was 3C 41, with polarimetry in 3 bands: $P_V = 9.3 \pm 2.3$ per cent; $P_H = 6.6 \pm 1.6$ per cent; $P_K = 3.1 \pm 1.1$ per cent. We attempted to fit two models; an electron model and a typical dust model with a minimum grain radius of 80 nm. To fit the models to the observed polarizations, we tested a discrete series of possible spectral indices, $-0.5 \leq \alpha \leq 2$, with a step size of $1/3$. For each value of α we calculated the ‘unscaled polarizations’ $\Pi_V \pm \epsilon_V$, $\Pi_H \pm \epsilon_H$, $\Pi_K \pm \epsilon_K$. We then iteratively determined the best fit value of C for each α , and took as our overall best fit that combination of α and C which gave the lowest δ .

Magnitudes for 3C 41 were available in 5 bands: J, H and K (Lilly & Longair 1984) and the narrow filters g and r_S (Dickinson, private communication). The H and K values yielded direct estimates of the corresponding ‘unscaled polarizations’ Π_H and Π_K ; Π_V was estimated by linear interpolation between Π_g and Π_{r_S} .

Figure 4 shows the measured polarizations for 3C 41 as triangles (\blacktriangle) and the magnitude-based polarization estimates, after best-fit scaling, as stars (\star). The lines give the error envelope on the modelled polarization (based only on

the errors on the magnitudes). The solid lines correspond to the dust model, and the dashed lines to the electron model.

As can be seen from Figure 4, the model curves lie below the data point at H, but above those at K and V. The shape of the curve depends more strongly on the measured magnitudes (and on f_W for dust) than on the spectral index, and the models for all reasonable values of α will have a broadly similar shape; the best fit will necessarily pass below the measured point at H, and above that at V.

Consider the electron model. Figure 4 shows us that the theoretical polarization curve for electron scattering is concave with respect to the origin, whereas a curve through the three data points would be convex; clearly it will not be possible to obtain a close fit for the central (H-band) point. Fitting the electron model curve, we found that the best fit occurred for $\alpha = 1.733$, with a deviation $\delta = 0.430$. From Table 4, we have $\Phi_K = 6 \pm 4$ per cent for 3C 41. Multiplying the polarizations observed at H and V by $1/P_{Q,W} = 2 \pm 1$, we predict $\Phi_H = 13 \pm 7$ per cent, and $\Phi_V = 19 \pm 10$ per cent in these bands.

The dust model chosen as typical from MdSA was that for a cloud of spherical dust grains, with radii $250 \text{ nm} > a > 80 \text{ nm}$, with the number density per unit dust mass following an $a^{-3.5}$ law. This model produced a curve which fitted the data points very well. The best fit indicated that the optimum spectral index was $\alpha = 1.167$, for which $\delta = 0.177$.

This dust model was also used to estimate the proportion of scattered light at shorter wavelengths: $\Phi_K = 8 \pm 4$ per cent, $\Phi_H = 24 \pm 6$ per cent, and $\Phi_V = 155 \pm 38$ per cent. MdSA’s curve for polarization as a function of rest-frame wavelength predicts a 6 per cent polarization in the observed V-band, lower than the 9 per cent *after dilution* measured by Jannuzi (private communication) (Elston & Jannuzi 1997). This is still consistent, within error bars, as long as the true value of Φ_V for 3C 41 is less than, but very close to, unity; the observed V-band corresponds to the near-ultraviolet in the rest frame of 3C 41, and it is reasonable (MdSA) to suppose that the scattered quasar light in that band could form in excess of eighty per cent of the total light.

We noted earlier that the shape of the dust model polarization curve between $0.2 \mu\text{m}$ and $0.7 \mu\text{m}$ (rest frame) is very sensitive to the choice of dust grain distribution. The particular dust model chosen approaches zero polarization at a wavelength corresponding to the r_S band when redshifted into our frame. This causes the ‘well’ visible in the model polarization curve (Figure 4), whose presence is essential for the dust model curve to fit the data points closely.

We also considered other dust models from the selection given by MdSA. Of those which differed significantly from the ‘typical’ one considered so far, many of them will not predict polarizations in the observed V-band which are sufficiently high to be reconciled with the observed 9 per cent; and those which do, do not possess the deep well needed to fit the polarimetry across the spectrum. We conclude, therefore, that the best model for 3C 41 is that of an obscured quasar core with $\alpha \sim 1.2$ beaming its optical radiation into a dust cloud, although an electron model cannot be ruled out within the error bars.

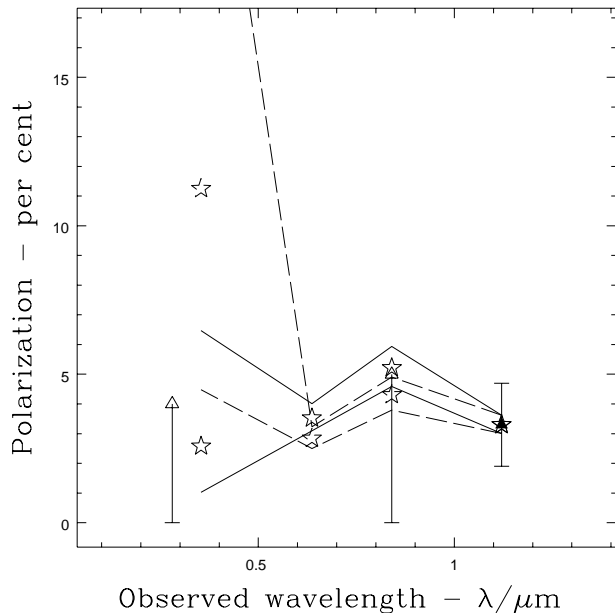


Figure 5. Modelled ($\alpha = 1$) and measured polarizations of 3C 22 as a function of rest-frame wavelength. Solid line: dust model; dashed line: electron model.

A model for 3C 22

For 3C 22, we have one firm polarimetry point (this paper) and two upper limits in V and H (Jannuzi, private communication) (Elston & Jannuzi 1997); magnitudes were available in 4 bands including J, H and K (Lilly & Longair 1984), and a crude eye estimate in r (Riley, Longair & Gunn 1980). The measurements and models are shown in Figure 5, with the same symbols as Figure 4; open triangles represent upper limits. We have taken $\alpha = 1$, and normalised the theoretical curves to the K-band data point.

Here the models are inconclusive. In the observed near-infrared, both models can easily fit, with some slight scaling, within the K-band measurement error bars; both models suggest that about 8 per cent of the K-band light arises in the active nucleus (Table 4). The error on the observed r-band magnitude is so large that both models are consistent with the observed V-band upper limit of polarization.

5 CONCLUSIONS

We have taken K-band polarimetry for seven 3CR radio galaxies, and found a diverse range of results. Out of our seven sources, two (3C 65 and 3C 441) display no evidence for polarization. For the five sources which do display some evidence of polarization, we have estimated the fraction of observed K-band light which originated in the active nucleus.

The recent finding (Eales et al. 1997) that 3C galaxies at $z \sim 1$ are 1.7 times as bright as the radio-weaker 6C/B2 galaxies in a similar sample requires that $\Phi_K \gtrsim 40$ per cent ($= 7/17$) for 3C galaxies, if the scattering of nuclear nonstellar light is responsible for the brighter K-band magnitudes of 3C galaxies. Our results suggests that Φ_K is somewhat lower. Nevertheless, our results support the hypothesis that

radio galaxies consist of quasar nuclei embedded in giant elliptical galaxies.

All of the galaxies which appear to be polarised have large errors on the orientation of the \mathbf{E} -vector; hence any apparent alignment effects are suggestive rather than definitive. But with this caveat, we note that two sources (3C 54 and 114) display extended K-band structure, and have high polarizations oriented in roughly parallel alignment with the radio axis and extension of the optical structure – i.e., in the opposite sense to the perpendicular alignment expected under a simple scattering model.

Finally, 3C 22 and 3C 41 display significant polarization of around 3 per cent, with a polarization alignment perpendicular to their radio axes; both appear in K-band as pointlike objects. We suggest, therefore, that in these objects, infrared light from a quasar core is being scattered into our line of sight, and forms a significant part of the total K-band flux received from these sources.

Manzini & di Serego Alighieri (MdSA) comment that given the range of possible dust models, ‘the wavelength dependence of polarization is not necessarily a discriminant between electron and dust scattering.’ The data available to us are insufficient to indicate whether the scattering centres in these objects are electrons or dust; it is not possible to give an unambiguous fit of the polarization curves with so few data points, although 3C 41 does seem to fit a model (MdSA) with a minimum dust radius of 80 nm, particularly well, and we suggest that it does indeed consist of a quasar obscured by dust.

Acknowledgements

We thank Steve Rawlings for his encouragement in this project; Colin Aspin and Tim Carroll for help with making the observations; Buell Jannuzi and Richard Elston for sharing their polarimetry results; Mark Dickinson for some optical magnitudes; and Jim Hough, Chris Packham and Antonio Chrysostomou for help with our polarimetry reduction. Simone Bianchi, Paul Alton, Bryn Jones, Bob Thomson, Neal Jackson, Arjun Dey, Clive Tadhunter and Patrick Leahy provided useful references. We also thank the anonymous referee for his constructive comments.

This research has made use of the NASA/IPAC extragalactic database (NED) which is operated by the Jet Propulsion Laboratory, CalTech, under contract with the National Aeronautics and Space Administration.

The United Kingdom Infrared Telescope is operated by the Joint Astronomy Centre on behalf of the U. K. Particle Physics and Astronomy Research Council. We thank the Department of Physical Sciences, University of Hertfordshire for providing IRPOL2 for the UKIRT. GL thanks PPARC for a postgraduate research student award.

REFERENCES

- Aspin C., 1994, IRCAM3 Operations Manual v1.07, Joint Astronomy Centre, Hilo, Hawaii; available on the World Wide Web at URL <http://www.jach.hawaii.edu/~caa/i3/i3.html>
- Aspin C., 1995, IRCAM3+IRPOL2 polarimetry data acquisition and reduction, Joint Astronomy Centre, Hilo, Hawaii; available on the World Wide Web at URL <http://www.jach.hawaii.edu/~caa/pol.doc>

- Chrysostomou A., 1996, Imaging Polarimetry with IRCAM3, Joint Astronomy Centre, Hilo, Hawaii; available on the World Wide Web at URL <http://www.jach.hawaii.edu/UKIRT/new/instruments/irpol/IRCAM/ircampol.html>
- Burstein D., Heiles C., 1982, *AJ*, 87, 1165
- Chambers K. C., Miley G. K., van Breugel W., 1987, *Nat*, 329, 604
- Cimatti A., di Serego Alighieri S., Fosbury R. A. E., Salvati M., Taylor D. N., 1993, *MNRAS*, 264, 421
- Clarke D., Stewart B. G., Schwarz H. E., Brooks A., 1983, *A&A*, 126, 260
- di Serego Alighieri S., Fosbury R. A. E., Quinn P. J., Tadhunter C. N., 1989, *Nat*, 341, 307
- Dickinson M., 1996, private communication
- Dunlop J. S., Peacock J. A., 1993, *MNRAS*, 263, 936
- Eales S. A., Rawlings S., Law-Green D., Cotter G., Lacy M., 1997, *MNRAS*, in press
- EGgen O. J., Lynden-Bell D., Sandage A. R., 1962, *ApJ*, 136, 748
- Elston R., Jannuzi B., 1997, *ApJL*, in preparation
- Fabian A. C., 1989, *MNRAS*, 238, 41P
- Hough J., 1996, private communication
- Jannuzi B., 1996, private communication
- Jannuzi B., Elston R., 1991, *ApJ*, 366, L69
- Koorneef J., 1983, *A&A*, 128, 84
- Leyshon G., 1997, Experimental Astronomy, submitted, 'On the reduction of astronomical photopolarimetry.'
- Lilly S. J., Longair M. S., 1984, *MNRAS*, 211, 833
- Longair M. S., 1975, *MNRAS*, 173, 309
- McCarthy P. J., van Breugel W., Spinrad H., Djorgovski S., 1987, *ApJ*, 321, L29
- Manzini A., di Serego Alighieri S., 1996, *A&A*, 311, 79
- Martin P. G., Whittet D. C. B., 1990, *ApJ*, 357, 113
- Mood A. M., Graybill F. A., Boes D. C., 1974, Introduction to the Theory of Statistics, third edition. McGraw-Hill
- Rawlings S., Lacy, M., Sivia D. S., Eales S. A., 1995, *MNRAS*, 274, 428
- Rieke G. H., Lebofsky M. J., 1985, *ApJ*, 288, 618
- Rigler M. A., Lilly S. J., Stockton A., Hammer F., LeFevre O. N., 1992, *ApJ*, 385, 61
- Rigler M. A., Lilly S. J., 1994, *ApJ*, 427, L79
- Riley J. M., Longair M. S., Gunn J. E., 1980, *MNRAS* 192, 233
- Savage B. D., Mathis J. S., 1979, *ARAA*, 17, 73
- Schilizzi R., Kapahi V. K., Neff S., 1982, *JAp&A*, 3, 173
- Schmidt-Kaler T., 1958, *Zs.f.Ap*, 46, 145
- Serkowski K., Matthewson D., Ford V., 1975, *ApJ*, 196, 261
- Simmons J. F. L., Stewart B. G., 1985, *A&A*, 142, 100
- Strom R. G., Riley J. M., Spinrad H., van Breugel, W. J. M., Djorgovski S., Liebert J., McCarthy P. J., 1990, *A&A*, 227, 19
- Tadhunter C. N., Scarrott S. M., Draper P., Rolph, C., 1992, *MNRAS*, 256, 53P
- Vinokur M., 1965, *Annales d'Astrophysique*, 28, 412
- Wardle J. F. C., Kronberg P. P., 1974, *ApJ*, 194, 249
- Wilking B. A., Lebofsky M. J., Martin P. G., Rieke G. H., Kemp J. C., 1980, *ApJ*, 235, 905